Product Vibrational State-to-State Correlation in the F + SiH_4 → HF(v_{HF}) + SiH_3 ($0v_20$) Reaction: A Crossed Molecular Beam Ion-Imaging Study†

Weiqing Zhang, Guorong Wu, Huilin Pan, Quan Shuai, Bo Jiang, Dongxu Dai, and Xueming Yang*

State Key Laboratory of Molecular Reaction Dynamics, Dalian Institute of Chemical Physics, Chinese Academy of Sciences, Dalian, Liaoning 116023, P. R. China

Received: December 27, 2008; Revised Manuscript Received: February 15, 2009

The dynamics of the F + SiH_4 → HF + SiH_3 reaction has been studied using the crossed molecular beam technique with slice imaging at collision energies from 1.25 to 8.17 kcal/mol. The product silyl radical, $SiH_3(v_2 = 0-5)$, was detected using the (2 + 1) resonance enhanced multiphoton ionization technique. The product velocity distributions and angular distributions of this reaction were obtained from the recorded images. Experimental results show that the silyl radical product is mainly forward scattered relative to the silane beam direction, and the majority of the available energy was partitioned into the vibration of the HF product. The state-to-state correlation between the two reaction products, SiH_3 and HF, was also determined. In addition, we found that the reaction cross section goes down as the collision energy increases. From these results, we conclude that the F + SiH_4 → HF + SiH_3 reaction proceeds through a direct abstraction mechanism with little or no reaction barrier.

1. Introduction

The reactivity of the silane molecule has been the subject of many experimental studies because of its importance in the semiconductor manufacturing and electronic industry. In the process of chemical vapor deposition (CVD), the reactions involving silane are essential to the quality of the deposited films. Kinetics and dynamics of these reactions have been extensively investigated. For example, the reaction rate constant of silane and an oxygen atom was measured by Ding and co-workers in 1993,[1] and the dynamics was investigated using the crossed molecular beam method in 2000.[2] Fluorine atom reactions with different species have also been extensively studied. The F-atom reaction with H_2 provided us an excellent example of reaction resonances,[3−9] while interesting dynamics of the F-atom reactions with methane,[10−13] ethylene,[14,15] propyne,[16] propene,[17] and other species[18−20] have been revealed in the crossed molecular beam scattering studies.

Similar to the F-atom reaction with methane, the F + SiH_4 → HF + SiH_4 reaction is exothermic with an exothermicity of 45.2 kcal/mol. In 1977, Smith and co-workers measured the rate constant of F + SiH_4 using the HF infrared chemiluminescence method at room temperature.[21] From this work, the reaction rate of F + SiH_4 was found to be about 7 times faster than that of F + CH_4, and the product HF from this reaction was clearly vibrationally excited. In 2006, Shen and co-workers carried out crossed molecular beam scattering studies of the F-atom reaction with SiH_4 using the universal crossed molecular beam method. [22] Two different channels, HF + SiH_3 and SiH_3F + H, have been observed in this reaction. Experimental results indicated that the HF product of the HF + SiH_3 channel is predominantly forward scattered relative to the F-atom beam direction, whereas the SiH_3F product of the SiH_3F + H channel is backward scattered, relative to the F-atom beam direction, suggesting that two reaction channels occur with very different reaction mechanisms. The SiH_3F + H channel takes place seemingly via a typical S_N2-type reaction mechanism, while the HF + SiH_3 reaction channel proceeds via a direct harpoon-type abstraction mechanism that produces a forward scattering product distribution. The relative branching ratios of the two channels was estimated to be 61% to 39% for HF + SiH_3 and SiH_3F + H, respectively. In the above studies, no vibrational state resolved information was obtained for both channels.

In the recent years, crossed molecular beam technique combined with the slicing ion velocity mapping method has been proved to be an extremely powerful tool for investigating the dynamics of polyatomic reactions, especially X (= F, Cl, O) + CH_4 reactions.[23−25] Interesting dynamics in the F-atom reaction with methane has been observed, providing an excellent example of state-to-state correlation in a polyatomic chemical reaction. In this work, we would like to report our recent experimental results on the HF + SiH_3 channel in the F-atom reaction with silane using a newly developed, crossed-beams slicing imaging apparatus. The SiH_3 product at specific vibrational states was detected via a (2 + 1) resonance enhanced multiphoton ionization (REMPI) technique.[26] By measuring the vibrational state specific product (SiH_3) ion velocity images, the correlated HF product vibrational state distributions were clearly determined. From these measurements, the vibrational state-to-state correlated dynamics in the F + SiH_4 → HF + SiH_3 reaction were investigated in details.

2. Experimental Methods

The reaction of F + SiH_4 has been studied in our laboratory using the crossed molecular beam scattering technique with slicing ion imaging, in combination with REMPI detection. The experiments were carried on a newly developed apparatus that has been described in detail elsewhere.[27] The new crossed beams ion imaging apparatus has three vacuum regions: two beam source chambers and one reaction/detection chamber. One of

† Part of the "George C. Schatz Festschrift".

* To whom all correspondences should be addressed. E-mail: xmyang@dicp.ac.cn.

10.1021/jp8114429 CCC: $40.75 © 2009 American Chemical Society
Published on Web 03/19/2009

the source chambers is fixed, and the other one can be rotated from 60° to 180° relative to the fixed beam source so that collision energy can well controlled during the experiment. For the current experiment, the F-atom beam was generated by a double-stage pulsed discharge before the expansion of a premixed sample of F_2 (5%) and He (95%) (Spectra Gases Inc.)[28] or a premixed sample of NF_3 (50%), F_2 (2.5%), and He (47.5%) in the fixed source chamber. No contaminant that could affect the results has been found in the F-atom beam. The two samples were used to cover the difference collision energy range. The F-atom beam was led to the reaction chamber through a 1.5 mm diameter skimmer and was then crossed with a skimmed SiH_4 beam in the reaction chamber from the rotating source chamber. The SiH_4 molecular beam was generated by expanding a sample of 50% SiH_4 in Ar at a stagnation pressure of about 3 atm through a carefully adjusted pulsed valve (General Valve) with a risetime of about 50 μs. The silane beam was then skimmed once by a 1.5 mm orifice skimmer before entering the reaction chamber. The speed of the SiH_4 beam was about 680 m/s. The speed of the F-atom beam from the discharge of the premixed sample of F_2 (5%) and He (95%) was about 1900 m/s, whereas that from the discharge of the premixed sample of NF_3 (50%), F_2 (2.5%), and He (47.5%) was about 1000 m/s. The collision energy was varied by changing the crossing angle between the F-atom beam and the silane beam, as well as exchanging the two premixed samples for the F-atom beam. Using the premixed sample of NF_3 (50%), F_2 (2.5%), and He (47.5%), collision energy as low as 1.25 kcal/mol can be achieved with a beam crossing angle of 60°. Using the premixed sample of F_2 (5%) and He (95%), a collision energy of 8.17 kcal/mol can be reached with a crossing angle of 125° between the two beams.

The crossing region of two beams was located at the center of the ion-imaging optics. The reaction product, SiH_3, was detected by a (2 + 1) REMPI scheme via the $\tilde{E}^2A''_2$ (4p) Rydberg state.[26] The UV photon of 410−420 nm was generated by a YAG-pumped dye laser output. The typical UV pulse energy was 5−6 mJ, and a lens with a focal length of 43 cm was used to focus the laser beam into the crossing region. The SiH_3 product ion was velocity mapped to an imaging quality microchannel plate (MCP) detector. The ion imaging signal was coupled out via a phosphor screen and detected by a CCD camera. The image signal was then transferred to a computer and accumulated over a significant amount of laser shots. The total voltage of ion optics was held at 700 V, at which the whole image could be recorded. The turnaround time of the products ion packet was more than 200 ns at this voltage setting, and a slicing window of 30 ns was used for the SiH_3 product ions for proper slicing imaging. The 30 ns slicing window was sufficiently narrow for high resolution and 3D velocity distribution reconstruction.[29] The (2 + 1) REMPI spectrum of the SiH_3 product was recorded by a photomultiplier tube looking on the phosphor screen. During the experiments, the vacuum was maintained at about 1×10^{-5} torr in the source chambers and at about 4×10^{-7} torr in the detection chamber.

3. Results and Discussion

3.1. SiH_3 REMPI Spectrum. The (2 + 1) REMPI spectroscopy of the SiH_3 radical has been carefully studied by Hudgens and co-workers.[26] From the detailed REMPI spectra, it was found that the SiH_3 radical in the ground electronic state is pyramidal with its potential minimum at the angle of $\theta_m = 20.7°$, where θ is defined as the angle between the line through the Si−H axis and the plane formed from the three hydrogen atoms. The SiH_3 radical is similar to ammonia and has two potential energy minima along the C_3 axis, the umbrella mode coordinate, shown in Figure 1.[26] For a typical double-minimum potential, the vibrational levels below the potential barrier have collapsed into closely spaced doublet levels. The splitting of these levels are related the potential barrier height. Those levels above the barrier are well separated. The (2 + 1) REMPI spectrum for the SiH_3 radical has been measured and assigned by Hudgens and co-workers.[26] This is helpful for the current dynamical studies of the F + SiH_4 → HF + SiH_3 reaction. In this work, we have measured the REMPI spectrum of the SiH_3 radical product from the F + SiH_4 reaction. Figure 2 shows the (2 + 1) REMPI spectrum of the SiH_3 product from the F + SiH_4 reaction via the $\tilde{E}^2A''_2$ (4p) Rydberg state. The assignment of the REMPI spectrum of the SiH_3 radical was made according to Hudgens and co-workers. [26] From the REMPI spectrum, the SiH_3 product is only excited in the umbrella mode. Vibrational excited states up to $v_2 = 5$ in the umbrella mode are populated in the SiH_3 product from the F + SiH_4 reaction.

Using the (2 + 1) REMPI detection scheme, the SiH_3 product at specific vibrational states from the F + SiH_4 reaction can be efficiently detected. However, detection efficiency of SiH_3 at

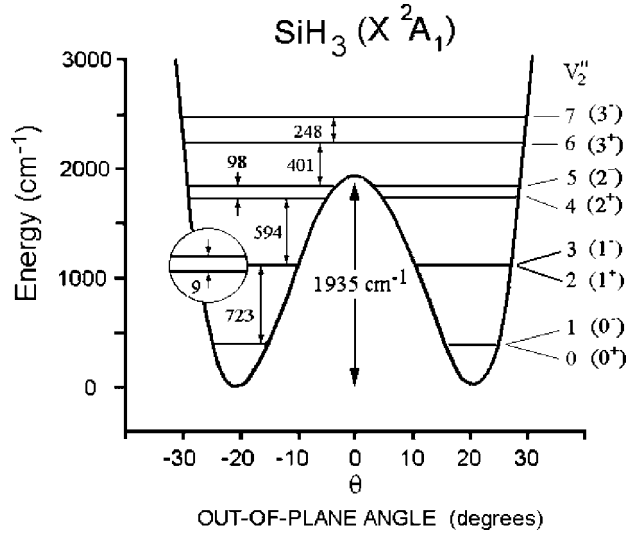

Figure 1. One-dimension, double minimum potential function of SiH_3 along the C_3 axis. This plot also shows v_2 umbrella vibrational levels of SiH_3 as a function of symmetric out-of-plane bending "umbrella" angle.

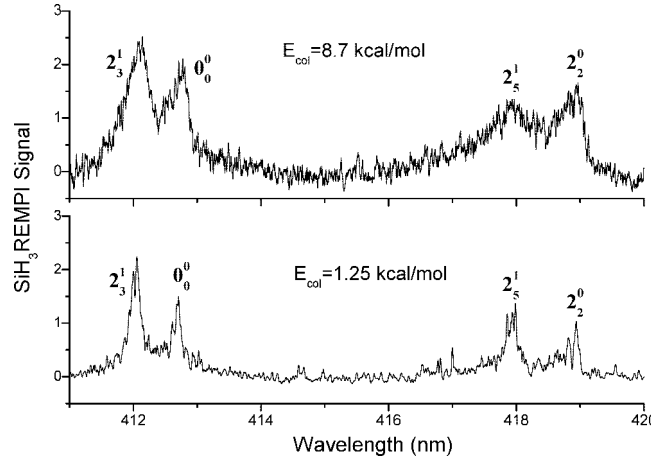

Figure 2. (2 + 1) REMPI spectra of the SiH_3 product via the $\tilde{E}^2A''_2$ (4p) Rydberg state at the collision energy of 1.25 and 8.17 kcal/mol.

different vibrational states are different, and therefore relative product populations of SiH_3 in different vibrational states cannot be quantitatively measured. From the REMPI spectra shown in Figure 2, the shapes of the different vibrational bands are different at different collision energies. At 1.25 kcal/mol, the vibrational bands are quite narrow, and the different bands are well separated from each other in the spectrum. At a higher collision energy of 8.17 kcal/mol, each vibrational band becomes broader. Consequently, the vibrational features become somewhat overlapped. These results indicate that the SiH_3 product is less rotationally excited at lower collision energy and significantly more rotationally excited at higher collision energy. From the relative integrated intensities of the different vibrational bands, we found that the higher vibrationally excited state of SiH_3 becomes relatively more important at higher collision energy, suggesting that the SiH_3 product vibrational excitation in the umbrella mode increases as the collision energy.

3.2. Reaction Product Images. Sliced velocity map ion images for the SiH_3 radical at different vibrational states were measured at different collision energies using the REMPI detection scheme since the first six vibrational levels in the umbrella mode in SiH_3 appear in pairs, $\upsilon_2 = 0$, 1, 2 and 3, 4, 5 with small energy difference. We have measured velocity ion images for each pair at the collision energy of 2.5 kcal/mol, and the images for the SiH_3 product at each pair vibrational levels are very similar. This suggests that the reaction dynamics producing the vibrationally excited SiH_3 products at these pair states are similar. Therefore, the data presented in this work are all based on the velocity map ion images of the SiH_3 product at $\upsilon_2 = 0$, 3, 5 states, which were detected through (2 + 1) REMPI at the wavelengths of 412.7, 412.0, 417.9 nm respectively. Figure 3 shows the typical raw images for the SiH_3 product at the $\upsilon_2 = 0$, 3, 5 levels at the collision energy of 2.5 kcal/mol. Two ringlike structures are well resolved in these images. From the well-known energetics of this reaction, these structures are assigned to the correlated HF product at $\upsilon' = 4$ (inner ring) and $\upsilon' = 3$ (outer ring). Clearly, the correlated HF product is produced exclusively in $\upsilon' = 3$ and 4 states. From the raw images, the SiH_3 product is also mainly forward scattered with respect to the SiH_4 beam direction. This result is consistent with the result of previous crossed beam studies of the same reaction using a universal molecular machine.[22] Similarly, the raw images for the SiH_3 product at two other collision energies, 1.25 and 8.17 kcal/mol, are also recorded.

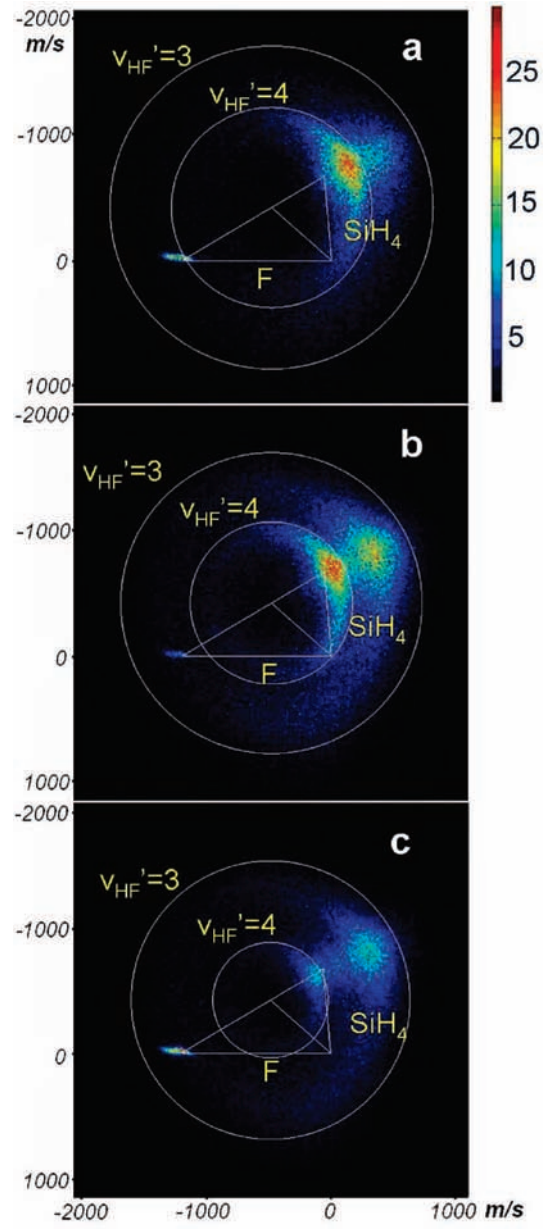

Figure 3. Raw images of the SiH_3 product at the collision energy of 2.5 kcal/mol: (a) $SiH_3(\upsilon_2 = 0)$; (b) $SiH_3(\upsilon_2 = 3)$; (c) $SiH_3(\upsilon_2 = 5)$.

3.3. Product Angular Distributions. In order to obtain the product velocity and angular distributions, the density-to-flux transformation is performed through an analysis program developed earlier.[27] Product angular distributions were obtained by integrating signals at the different angles in the density-to-flux transformed images. Figure 4 shows the total product angular distributions at three collision energies. At all three collision energies, the SiH_3 product is mainly forward scattered relative to the SiH_4 direction. This is also true for the SiH_3 product at different vibrational states. The angular distribution of the HF product at $\upsilon' = 3$ and 4 states are also clearly forward scattered, relative to the F-atom beam. The degree of the forwardness for the SiH_3 product is also different at different collision energies. At the collision energy of 1.25 kcal/mol, the reaction product is mainly forward scattered. However, there is a significant amount of product at the sideway and backward scattering directions. As the collision energy increases, the backward/sideway scattered product flux becomes smaller relative to that for the forward scattering direction. At the collision energy of 8.17 kcal/mol, backward scattering product becomes very small relative to the forward scattering product and the total product angular distribution is exclusively forward scattered. These results suggest that as the collision energy increases the product angular distribution becomes more forward scattered. For the SiH_3 product at different vibrational states, the angular distributions are also different. It seems that if the vibrational excitation of SiH_3 is smaller, the SiH_3 product is overall more forward scattered.

3.4. Product Velocity Distributions and State-to-State Correlation between HF and SiH_3. Through the density-to-flux transformation of the raw images, velocity distributions of the SiH_3 product can also be obtained. Figure 5 shows the velocity distributions of the SiH_3 product at $\upsilon_2 = 0$, 3, 5 obtained from the images at the collision energy of 2.5 kcal/mol. The curve contains two features, which can be assigned to the HF $\upsilon' = 3$ and $\upsilon' = 4$ levels. The relative branching ratios of HF($\upsilon' = 3$) and HF($\upsilon' = 4$) were determined by fitting the distributions using two components. The relative branching ratios obtained are listed Table 1. The relative branching ratios of the HF($\upsilon' =$

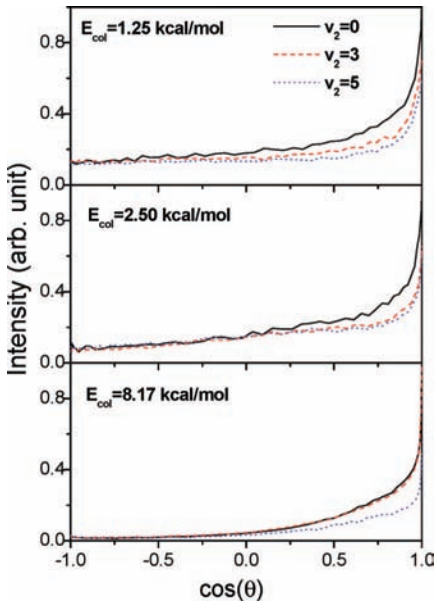

Figure 4. Angular distributions of the SiH_3 product with respect to the SiH_4 beam direction at 1.25, 2.5, and 8.17 kcal/mol. The black solid line is the result for $SiH_3(v_2 = 0)$, the red dashed line is for $SiH_3(v_2 = 3)$, and the blue dotted line is for $SiH_3(v_2 = 5)$.

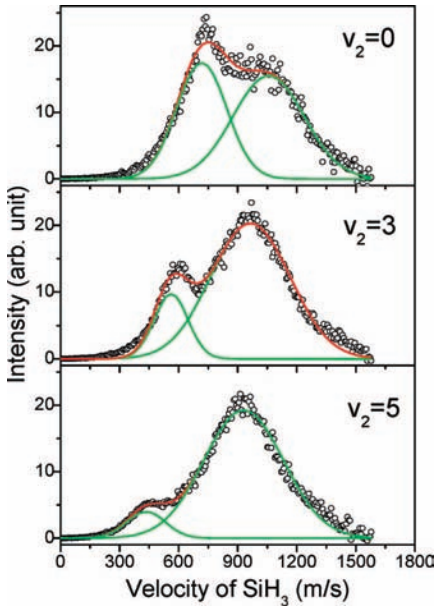

Figure 5. Velocity distributions of the SiH_3 product at 2.5 kcal/mol for SiH_3 at $v_2 = 0$, 3, and 5. The open circles in the figure are the experiment results, the green lines are simulated results for the correlated $v = 3$ and $v = 4$ HF products, and the red line is the total simulated result.

3) and HF($v' = 4$) products vary considerably for different vibrationally excited SiH_3 products. For the SiH_3 product at $v_2 = 5$, nearly all HF product is populated in the $v' = 3$ state, with very little in $v' = 4$ state (9%), whereas for the SiH_3 product at $v_2 = 0$, there is a considerable increase in the HF($v' = 4$) population (44%). From these results, there is clearly vibrational state-to-state correlation between the SiH_3 and HF products. The SiH_3 and HF products seem to be anticorrelated vibrationally. The higher the SiH_3 vibrational excitation, the lower the HF vibrational excitation. From the correlated images, we can also conclude that the rotational excitation of the HF($v' = 3$) product is significantly higher than that of the HF($v' = 4$) product. This is largely due to the different available energies of the two

TABLE 1: Averaged cos θ, Product Energy Disposals, and HF Vibrational Branching Ratios (All Energies in kcal/mol)

	$v_{SiH_3} = 0$	$v_{SiH_3} = 3$	$v_{SiH_3} = 5$
	$E_C = 1.25$		
$\langle \cos\theta \rangle$	0.23	0.18	0.15
$\langle E_T \rangle_{total}$	5.6	6.7	7.1
$\langle E_{v'} \rangle_{HF}$	36.3	33.8	32.7
$\langle E_{v'} \rangle_{SiH_3}$	0	2.1	4.1
$\langle E_{v'} \rangle_{total}$	36.3	35.9	36.8
$v_{HF} = 3$ (%)	62	87	100
$v_{HF} = 4$ (%)	38	13	0
	$E_C = 2.5$		
$\langle \cos\theta \rangle$	0.31	0.25	0.21
$\langle E_T \rangle_{total}$	8.2	8.2	8.2
$\langle E_{v'} \rangle_{HF}$	36.9	34.4	33.4
$\langle E_{v'} \rangle_{SiH_3}$	0	2.1	4.1
$\langle E_{v'} \rangle_{total}$	36.9	36.5	37.5
$v_{HF} = 3$ (%)	56	81	91
$v_{HF} = 4$ (%)	44	19	09
	$E_C = 8.17$		
$\langle \cos\theta \rangle$	0.56	0.54	0.48
$\langle E_T \rangle_{total}$	11.2	11.0	11.0
$\langle E_{v'} \rangle_{HF}$	39.2	36.6	34.6
$\langle E_{v'} \rangle_{SiH_3}$	0	2.1	4.1
$\langle E_{v'} \rangle_{total}$	39.2	38.7	38.7
$v_{HF} = 3$ (%)	31	59	78
$v_{HF} = 4$ (%)	69	41	22

microchannels. Obviously, the HF($v' = 3$) product has more product rotational states for energy disposal and the HF($v' = 4$) product has fewer.

As collision energy increases, the HF($v' = 4$) product channel becomes more and more important than the HF($v' = 3$) channel, while the HF($v' = 3$) channel is less important. This seems to be true for all measured SiH_3 vibrational channels. At the collision energy of 1.25 kcal/mol, the correlated HF product are all in the $v' = 3$ state with no population at all in the $v' = 4$ state for the SiH_3 ($v_2 = 5$) product channel. At the collision energy of 8.17 kcal/mol, the HF($v' = 4$) channel already accounts for 22% of all HF product for the same SiH_3 ($v_2 = 5$) channel. For the SiH_3 ($v_2 = 0$) channel, the branching ratio of the HF($v' = 4$) increases from 38% at 1.25 kcal/mol to 69% at 8.17 kcal/mol.

A rather remarkable observation is the large proportion of the available energy deposited into the vibration of the HF product in such a polyatomic reaction. From Table 1, more than 70% of the available energy is partitioned into the HF vibration. This means that the majority of the available energy in this reaction is deposited to the HF vibration. This extreme vibrational excitation is very likely produced via a peculiar extraction mechanism, in which the F atom abstracts an H atom from the silane molecule at a relatively large distance and then flies away. Such reaction mechanism can also explain the strong forward scattering of the reaction products, which is produced likely via abstraction at large impact parameters.

3.5. Collision Energy Dependence of the Total REMPI Signal. Integral cross sections (ICS) for the SiH_3 product at specific vibrational states were also measured for the title reaction. Figure 6 shows the measured total REMPI signal for SiH_3 at $v_2 = 0$, 3, 5 versus the collision energy. These data were measured by integrating the total SiH_3 REMPI ion signals when the REMPI laser was parked at a specific transition. The collision energy variation is achieved by both changing the crossing angle between the two beams from 65° to 90° and varying the mixing ratio of the 5% F_2/He gas and the NF_3 gas in a premixed gas sample. By varying this mixing ratio, the

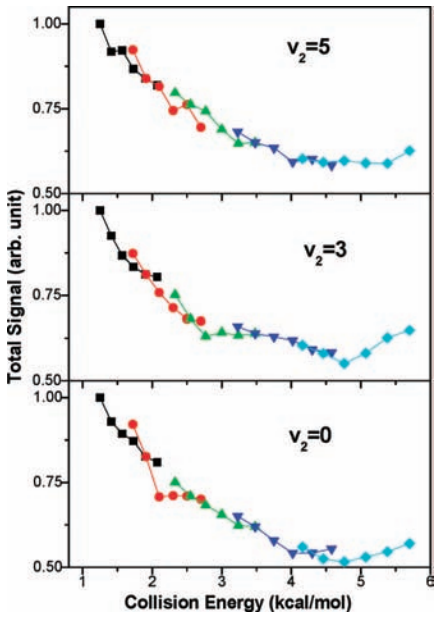

Figure 6. Relative integral cross section (ICS) as a function of the collision energy in the F + SiH_4 → HF + SiH_3 reaction for different vibrationally excited SiH_3 products.

F-atom beam velocity can be changed between 1000−2000 m/s. In this experiment, we have used a total of five different mixtures, in which the percentage of the NF_3 sample in the mixture are 50%, 25%, 16%, 10%, 0%, respectively. The collision energy for the F + SiH_4 reaction can be varied from 1.25 to about 5.7 kcal/mol with the beam crossing angle changing from 65° to 90° in addition to the gas mixture changes. The five measurements using different gas mixtures are put together by scaling the different sets of data to a single overlapping point. This allows us to the put together the whole total REMPI signal plots from 1.25 to 5.7 kcal/mol for specific vibrationally excited SiH_3 products at $v_2 = 0, 3, 5$. The total REMPI signal curves of the SiH_3 product in different vibrational state are very much similar. All curves decrease monotonically as the collision energy increases. Since the effects of the density-flux transformation and the relative velocity are somewhat similar at different collision energies, the trend of the total REMPI plots should be similar to that of the integral cross sections. Thus, we can conclude that the integral cross section for all reaction products should also decrease monotonically as the collision energy increases. This means that the F + SiH_4 → HF + SiH_3 reaction is likely a barrierless reaction governed by an attractive potential, which is quite consistent with the picture obtained from the product energy partitions.

4. Conclusions

In this work, we have investigated the dynamics of the F + SiH_4 → HF + SiH_3 reaction using the time-sliced velocity map ion imaging technique with (2 + 1) REMPI detection of the SiH_3 product. From the REMPI spectra of the SiH3 product, we found that the SiH_3 product is vibrationally excited only in the umbrella vibrational mode. Sliced raw images of the SiH_3 product at $v_2 = 0, 3, 5$ levels were acquired. After density-to-flux transformation of these raw images, both the velocity and angular distributions of the product SiH_3 at $v_2 = 0, 3, 5$ were obtained at three collision energies: 1.25, 2.50, and 8.17 kcal/mol. From the experimental results, we found that the majority of the available reaction energy is partitioned into the vibration degrees of freedom in the HF and SiH_3 products. Vibrational state distributions of the correlated HF product can be determined for the SiH_3 product at various vibrationally excited states. Therefore, information on the vibrational state-to-state correlation between the SiH_3 and HF products can be derived. From these results, vibrational state distributions for the SiH_3 and HF products are clearly anticorrelated. In addition, we found that the SiH_3 product at $v_2 = 0, 3, 5$ vibrational states are clearly forward scattered. At the low collision energy, the SiH_3 product has a large forward scattering peak, and backward and sideway scatterings are also significant. As the collision increases, however, the product angular distribution becomes more forward scattered. The integral cross sections for the SiH_3 product at $v_2 = 0, 3, 5$ states have been measured and obviously decrease monotonically as the collision energy increase. These results suggest that the F + SiH_4 → HF + SiH_3 reaction proceeds via a direct abstraction mechanism with little or no barrier.

Acknowledgment. This work was supported by the Chinese Academy of Sciences, the National Natural Science Foundation of China, and the Ministry of Science and Technology of China. We would also like to thank Prof. Kopin Liu for many helpful discussions. W.Z. and G.W. made similar contributions to this work.

References and Notes

(1) Ding, L.; Marshall, P. *J. Chem. Phys.* **1993**, *98* (11), 8545.
(2) Lin, J. J.; Lee, Y. T.; Yang, X. *J. Chem. Phys.* **2000**, *113* (5), 1831.
(3) Skodje, R. T.; SkooutersV, D.; Manolopoulos, D. E.; Lee, S.-H; Dong, F.; Liu, K. *J. Chem. Phys.* **2000**, *112*, 4536; *Phys. Rev. Lett.* **2000**, *85*, 1206.
(4) Neumark, D. M.; Wodtke, A. M.; Robinson, G. N; Hayden, C. C; Lee, *Phys. Rev. Lett.* **1984**, *53*, 226; *J. Chem. Phys.* **1985**, *82*, 3045.
(5) Qiu, M.; Ren, Z.; Che, L.; Dai, D.; Harich, S. A.; Wang, X.; Yang, X. *Chin. J. Chem. Phys* **2006**, *20*, 1.
(6) Qiu, M.; Ren, Z.; Che, L.; Dai, D.; Harich, S.; Wang, X.; Yang, X.; Xu, C.; Qian, D.; Gustafsson, M.; Skodje, R. T.; Sun, Z.; Zhang, D. H. *Science* **2006**, *311*, 1440.
(7) Qiu, M.; Ren, Z.; Che, L.; Dai, D.; Harich, S. A.; Wang, X.; Yang, X.; Xu, C.; Xie, D.; Gustafsson, M.; Skodje, R. T.; Sun, Z.; Zhang, D. H. *Science* **2006**, *311* (5766), 1440.
(8) Che, L.; Ren, Z. F.; Wang, X. G.; Dong, W. R.; Dai, D. X.; Wang, X. Y.; Zhang, D. H.; Yang, X. M.; Sheng, L. S.; Li, G. L.; Werner, H. J.; Lique, F.; Alexander, M. H. *Science* **2007**, *317* (5841), 1061.
(9) Yang, X.; Zhang, D. H. *Acc. Chem. Res.* **2008**, *41* (8), 981.
(10) Harper, W. W.; Nizkorodov, S. A.; Nesbitt, D. J. *J. Chem. Phys.* **2000**, *113*, 3670.
(11) Harper, W. W.; Nizkorodov, S. A.; Nesbitt, D. J. *Chem. Phys. Lett.* **2001**, *335*, 381.
(12) Lin, J. J.; Zhou, J.; Shiu, W.; Liu, K. *Science* **2003**, *300*, 966.
(13) Zhou, J.; Lin, J. J.; Shiu, W.; Pu, S.-C.; Liu, K. *J. Chem. Phys.* **2003**, *119*, 4997.
(14) Parson, J. M.; Lee, Y. T. *J. Chem. Phys.* **1972**, *56*, 4658.
(15) Robinson, G. N.; Continetti, R. E.; Lee, Y. T. *J. Chem. Phys.* **1990**, *92*, 275.
(16) Ran, Q.; Yang, C.-H.; Shen, G.; Lee, Y. T.; Yang, X. *J. Chem. Phys.* **2005**, *122*, 044307.
(17) Ran, Q.; Yang, C.-H.; Shen, G.; Lee, Y. T.; Yang, X. *J. Chem. Phys.* **2004**, *121*, 6302.
(18) Shobatake, K.; Lee, Y. T.; Rice, S. A. *J. Chem. Phys.* **1973**, *59*, 1453.
(19) Shobatake, K.; Parson, J. M.; Lee, Y. T.; Rice, S. A. *J. Chem. Phys.* **1973**, *59*, 1416.
(20) Parson, J. M.; Shobatake, K.; Lee, Y. T.; Rice, S. A. *J. Chem. Phys.* **1973**, *59*, 1402.
(21) Smith, D. J.; Setser, D. W.; Kim, K. C.; Bogan, D. J. *J. Phys. Chem.* **1977**, *81* (9), 898.
(22) Shen, G.; Yang, X.; Shu, J.; Yang, C.-H.; Lee, Y. T. *J. Chem. Phys.* **2006**, *125* (13), 133103.
(23) Lin, J. J.; Zhou, J.; Shiu, W.; Liu, K. *Rev. Sci. Instrum.* **2003**, *74* (4), 2495.
(24) Lin, J. J.; Zhou, J. G.; Shiu, W. C.; Liu, K. P. *Science* **2003**, *300* (5621), 966.
(25) Huang, C.; Li, W.; Suits, A. G. *J. Chem. Phys.* **2006**, *125* (13), 133107.
(26) Johnson, R. D., III; Tsai, B. P.; Hudgens, J. W. *J. Chem. Phys.* **1989**, *91* (6), 3340.

(27) Wu, G.; Zhang, W.; Pan, H.; Shuai, Q.; Jiang, B.; Dai, D.; Yang, X. *Rev. Sci. Instrum.* **2008**, *79* (9), 094104.
(28) Ren, Z.; Qiu, M.; Che, L.; Dai, D.; Wang, X.; Yang, X. *Rev. Sci. Instrum.* **2006**, *77* (1), 016102.
(29) Shiu, W.; Lin, J. J.; Liu, K.; Wu, M.; Parker, D. H. *J. Chem. Phys.* **2004**, *120* (1), 117.

JP8114429